Urban Heat Island Amplification Estimates on Global Warming Using an Albedo Model

Alec Feinberg
DfRSoft Research, email: dfrsoft@gmail.com, ORCID: 0000-0003-4364-2460

Abstract: In this paper, we provide nominal and worst-case estimates of radiative forcing due to the UHI effect using a Weighted Amplification Albedo Solar Urbanization (WAASU) model. This calculation is done with the help of reported findings from UHI footprint and heat dome studies that simplify estimates for UHI amplification factors. Using this method, we quantify a global warming range due to the UHI effect, including its extent. Forcing estimates varied approximately between 0.07W/m^2 to 0.87W/m^2 representing 3% to 36% of global warming (GW) relative to the greenhouse gas (GHG) forcing estimates between 1950 and 2019. Variations in our model are due to the urbanized area and associated UHI amplification estimate uncertainties. However, the model showed consistent values of about 0.16 W/m^2/% solar effective amplified areas and 1.6 W/m^2/%Δalbedo for the urbanized coverage forcing values. The basic model is additionally used to quantify feedback warming due to Arctic sea ice loss. Feedback estimates help put an assessment on UHI forcing implications. Results provide insight into the UHI area effects from a new perspective using a global view albedo model compared to prior ground-based measurement studies. It also illustrates the utility of using effective UHI amplification estimates when assessing UHI's warming effect on a global scale.

Keyword: Urban Heat Islands, Albedo Modeling, UHI Amplification Effects, UHI Heat Dome, Cool Roofs, Sea Ice Warming

1 Introduction

There are few recent publications about possible UHI influences on global warming. Thus, more up-to-date related studies, including UHI amplification effects that will be discussed in this paper, could offer supporting data for climate change theories and solutions.

One key paper often referred to is by McKitrick and Michael's [1,2], who found in 2004 and 2007 using regression trends on socioeconomic, geographical, and temperature indicators, that the net warming bias at the global level may explain as much as half the observed land-based warming. Another independent study often quoted by De Laat and Maurellis [3] in 2006 found very similar results. In 2007, IPCC [4] questioned these findings stating *"the locations of greatest socioeconomic development are also those that have been most warmed by atmospheric circulation changes, which exhibit large-scale coherence."* Therefore, inferring that correlation to warming was not statistically significant but a result of atmospheric oscillations. In 2009, Schmidt [5] agreed and published a paper also suggesting that McKitrick and Michael's observed correlations were probably spurious. However, in 2010, McKitrick responded with two publications, the first [6] entitled, "Atmospheric Oscillations do not Explain the Temperature-Industrialization Correlation." The second by McKitrick et al. in 2010 [7] detailed that, "evidence for contamination of climatic data is robust across numerous data sets...Consequently, we conclude that important data products used for the analysis of climate change over global land surfaces may be contaminated with socioeconomic patterns related to urbanization and other socioeconomic processes." In 2013, the IPCC summarized the controversy saying [8], "it is indisputable that UHI and land-use/land-cover are real influences on raw temperature measurements. At question is the extent to which they remain in the global products." Citations and discussions in the IPCC report suggested the UHI effect would not be more than 10% of observed warming.

However, other authors have also found UHI significance [9-17]. For example, Zhao and Huang et al. [14, 16] found that UHIs contributed to warming in China by about 30%. Bian et al. [17] in China at a Shijiazhuang station for periods 1965-2012 found the urban-rural land surface temperatures (LST) trends correlated 100% to urbanization contributions indicating the yearly increase in annual mean LST at the urban station is entirely caused by urbanization. They concluded the true impact of rising atmospheric CO_2 on the global climate may well be vastly overstated. These studies used land-based temperature station data to make assessments. It is further interesting to note that most of these studies [1-3, 9-16] infer that warming due to feedback is included indicating percentages relative to total forcing are likely higher. To date, one can conclude that all such studies and findings were not persuasive enough to be influential in the 2015 Paris Climate Accord [18] regarding the need for UHI albedo controls as part of the world-wide effort to mitigate global warming.

This paper provides insight into these controversial findings [1-3, 6-7, 9-17] with a WAASU model applied to two time periods, 1950 and 2019. There are currently no papers on the influence of urbanization on climate change using albedo modeling. However, this paper is restricted to UHI and its extent and does not take into account all forms of human land contamination (roads, rural human habitation, deforestation, evapotranspiration loss, anthropogenic heat release, etc.) of which should be roughly correlated in McKitrick and Michael's socioeconomic - geographical pattern analysis. In this respect, our results are likely conservative.

(Keywords are moved by viXra Admin to conform with scholaly norm)

The WAASU model has advantages as it works from a global view rather than with ground-based studies. There are no concerns about warming oscillations or GHG interference. The model is non-probabilistic and in line with typical energy budgets (IPCC, Hartmann et al. [8]). The model uses only two key parameters: normalized solar effective amplified area and weighted albedo values. Because it is simplistic, it has transparency compared with the complex land-based studies. We also show its utility by extending it to a Weighted Albedo Solar (WAS) model for global warming estimates due to arctic ice melting in Appendix D.

The contention that UHI effects are primarily of local significance is most likely related to urban area estimates. For example, the IPCC (Satterthwaite et. al. [19]) AR5 report references a Schneider et al. [20] study that resulted in urban coverage of 0.148% of the Earth (Table 1). This seemingly small area tends to dismiss the role that the UHI effect can play in large-scale global warming. Furthermore, estimates of how much land has been urbanized vary widely in the literature, in part due to the definition of what is urban and the datasets used. Although, such estimates are important for environmental studies, obtaining true estimates for the small urbanized area relative to the total land is very difficult. Compounded by the fact that there is a significant difference in how groups define the term "urban," Table 1 illustrates several variations from select papers of interest.

Table 1. Urbanization area extent estimates from various sources

Percent of Land	Percent of Earth	References
2.7	0.783	Global Rural Urban Mapping Project (GRUMP) [21] – using NASA satellite light studies based on 2004 data and with census data
1	0.29	NASA [22], Galka [23] – from satellite data
0.51	0.148	Schneider et al. [20] – based on 2000-2001 data and referenced in the IPCC report (Satterthwaite, [19])
0.5	0.145	Zhou [24] – based on a 2000 data set

Also, global warming UHI amplification effects have not been quantified to a large degree related to area estimates. Urbanized average solar areas remain unknown.

In our study, one key paper listed in Table 1 is that due to Schneider et al. [20] since it is cited by the AR5 2014 IPCC report (Satterthwaite et al. [14]). In Schneider's paper, the larger area found in the GRUMP [21] study (Table 1) is criticized. Nevertheless, we incorporate the GRUMP area as an upper bound. We note that UHI effects have been shown to arise even at very low levels of populations, i.e., towns with fewer than 10,000 people as noted by Karl et al., 1988 [25] and Chagnon 1999 [26]. The GRUMP study describes datasets with populations greater than 5,000 people while in the Schneider paper population estimates were not included. The GRUMP study combines population statistics and nightlights where the Schneider paper uses a high resolution of illuminated satellite data with decision tree algorithms.

Therefore, we use both the Schneider et al. and GRUMP studies for the minimum nominal and maximum worst-cases urbanization area estimates respectively. Furthermore, they were done using data sets near the year 2000, a reasonable point in time to extrapolate down to 1950 and up to 2019 (see Sec. 2.5), the two periods of this study.

1.1 UHI Amplification Effects

The table below lists key global warming causes and amplification effects. In general, the complex UHI amplification effects are responsible for the local thermal and related UHI global warming forcing issues. Propagating UHI global warming could further escalate the Earth's climate feedback response [27-29] (see the conclusion). A summary is provided in Appendix B of the key UHI effects listed in the table. As well Appendix B includes a discussion on how UHI effects can contribute to climate change issues.

Table 2. Global warming cause and effects

Global Warming Causes →	Population → Expanding Urban Heat Islands (UHI), Roads & Increases in Greenhouse Gas (GHG)
Global Warming Feedback Amplification Effects →	Water-Vapor Feedback, Land Albedo Change Due to Cities & Roads, Ice and Snow –Albedo Feedback, Lapse Rate Feedback, Cloud Feedback, etc.
Urban Heat Island Solar Amplification Effects →	UHI Solar Heating Area (Building Areas), UHI Building Heat Capacities, Humidity Effects, Hydro-Hotspots, Reduced Wind Cooling, Solar Canyons, Loss of Wetlands, Increase in Impermeable Surfaces, Loss of Evapotranspiration Natural Cooling.

2 Data and Methods

The Earth's solar area has physically increased since 1950 due to tall UHI building side area increases. The actual increase in UHI heat intensity though incorporates all solar factors described in Table 2. Besides the tall building solar sides, as shown in the table, many solar effects create the large amplified heat issue. This is a nonlinear problem that could be perhaps impossible to model and is likely best measured instead with what is called the UHI "Footprint" (FP) area, for example. In the discussion below, authors have found that the FP correlates to UHI actual area. Therefore in this section, we expand upon the FP concept. The FP was defined as the continuous extent emanating outward from urban centers to rural areas that have evident UHI effect (i.e., $\triangle$T was statistically larger than zero).

2.1 UHI Area Amplification Effect

We are interested in assessing what we term as the UHI complex solar amplification factor. This will only be applied to the UHI component in the WAASU model as an additional weighting factor. To determine this factor, it is logical as we discussed to first look at UHI FP studies as they provide a measure of the UHI amplified heat intensity. Zhang et al. [30] found the ecological FP of the urban land cover extends beyond the perimeter of urban areas, and the FP of urban climates on vegetation phenology they found was 2.4 times the size of the actual urban land cover. In a more recent study by Zhou et al. [31], day-night cycle temperature difference measurements were performed in China. In this study, they found the UHI effect decayed exponentially toward rural areas for the majority of the 32 Chinese cities. Their comprehensive study spanned from 2003 to 2012. They describe China as an ideal area to study since it has experienced the most rapid urbanization in the world in the decade they evaluated. They found that the FP of the UHI effect, including urban areas, was 2.3 and 3.9 times that of urban size for the day and night, respectively. We note that the average day-night amplification footprint coverage factor is 3.1.

To provide some assessment of how the UHI amplification factor scales, we note that Zhou et al. [31] found the FP physical area (km^2), correlated tightly and positively with the actual urban area having a correlation coefficient higher than 79% over 32 cities. This correlation suggests that area can be used to provide an initial estimate of this complex amplification factor. Furthermore, the fact that the amplification factor scales with the area is consistent in the calculation of the WAASU model that is weighted by area. This is discussed in Appendix A and Sec. 2.5 (Eq. 9).

Therefore, as a model assumption, it is reasonably justified that the amplification factor (AF) should scale with the ratio of areas from 1950 to 2019,

$$AF_{UHI\ for\ 2019} = \frac{\sum(UHI\,Area)_{2019}}{\sum(UHI\,Area)_{1950}} \tag{1}$$

Area estimates have been obtained in the next Section in Table 3 between 1950 and 2019 time frames, yielding the following results for the Schneider et al. [20] and the GRUMP [21] extrapolated area results:

$$AF_{UHI\ for\ 2019} = \frac{(Urban\,Size)_{2019}}{(Urban\,Size)_{1950}} \approx \begin{cases} \left(\frac{[0.188]_{2019}}{[0.059]_{1950}}\right)_{\text{Schneider}} = 3.19 \\ \left(\frac{[0.952]_{2019}}{[0.316]_{1950}}\right)_{GRUMP} = 3.0 \end{cases} \tag{2}$$

From the two studies, area scaling for the UHI solar amplification effect averages 3.1. Coincidently, this factor is the same observed in the Zhou et al. [31] study for the average footprint. This factor may seem high. However, it is likely conservative as other effects would be difficult to assess: increases in global drought due to loss of wetlands, deforestation effects due to urbanization, drought-related fires, and humidity issues. Also difficult to model are factor changes of other impermeable surfaces since 1950, such as city highways, parking lots, event centers, and so forth.

The 3.1 factor is one of the values used to weight the effective UHI area in the WAASU model between 1950 and 2019. It is applied as an UHI effective amplified solar (EAA_{UHI}) area giving more weight to the UHI albedo term. It

is initially applied to the UHI area in Table 3 with an example given in Equation 5. Appendix A and Equation 9 describe the EAA_{UHI} concept.

2.2 Alternate Method Using the UHI's Dome Extent

An alternate approach to check the estimate of Equation 3 is to look at the UHI's dome extent. Fan et al. [32] using an energy balance model to obtain the maximum horizontal extent of a UHI heat dome in numerous urban areas found the nighttime extent of 1.5 to 3.5 times the diameter of the city's urban area (2.5 average) and the daytime value of 2.0 to 3.3 (2.65 average). The horizontal extent of the heat dome is an important parameter for estimating the size of the area it influences and is similar to Zhou et al. [30] footprint.

In the Fan et al. method, the city diameter is multiplied by their derived day (2.65) and night (2.5) factors to obtain the horizontal extent. In our case, we want the diameter change from the area increase in Eq. 2, which is $1.8 (=\sqrt{3.1})$. Therefore, this yields 2.5 x 1.8=4.5 higher in the night and 2.65 x 1.8=4.8 in the day in 2019 with an average of 4.65. According to Fan et al. this occurs 62.5% of the time (their study indicated that transition states are 4 hours around sunrise, and about 5 hours around sunset, and had less effect, totaling 9 hours out of 24). This yields an effective horizontal extent UHI amplification factor of 2.9. We note this is in good agreement with Zhou et al. footprint and Eq. 2. Fan et al. [32] assessed the heat flux over the urban area extends to its neighboring rural area where the air is transported from the urban heat dome flow. Therefore the heat dome extends similarly as observed in the footprint studies. If we use the dome concept, we can assume that the actual surface area for the heat flux is increased as the surface area of the dome. This should be considered a measure of the atmospheric UHI vertical and horizontal extents which both are influential in global warming. We do not know the true diameter of the dome, but it is larger than the assessment by Fan et al. Using their dome extend applied to the area diameter D increase from 1950 to 2019, the amplification factor should be correlated to the ratios of the dome spherical surface areas:

$$AF_{UHI\ for\ 2019} = \left(\frac{D_{2019}}{D_{1950}} \right)^2 = 2.9^2 = 8.4 \tag{3}$$

This value is our second model assumption. Here the ratios of the dome's surface area are applied as an alternate approach in estimating how the amplification effect scales with UHI growth which provides a measure of vertical and horizontal extent. Therefore, we use both, 3.1 and 8.4, as upper and lower bounds for the solar EAA_{UHI}.

2.3 Applying the Amplification Factors

In this analysis, 1950 is the reference year. Therefore, it is not subjected to amplification. Only the new UHI solar area is amplified as we are looking at changes since this time frame. The EAA_{UHI} in 2019 (see Sec. 2.5) can then be defined as

$$EAA_{UHI} = AF_{UHI}\ x\ New\ area + Area_{1950} = AF_{UHI}\ x\ (Area_{2019} - Area_{1950}) + Area_{1950} \tag{4}$$

Using this, if there were no changes in UHI solar growth, for example, so that the $Area_{2019}=Area_{1950}$, the resulting area is just the original $Area_{1950}$ and if $AF_{UHI}=1$, yields the 2019 unamplified area. This result is applied to the new area in Table 3 below.

2.4 Area Extrapolations for 1950 and 2019

To assess the urbanized area, (also used in determining the UHI amplification factor ratios above), we need to project the Schneider [20] and GRUMP [21] area estimates down to 1950 and up to 2019. Both use datasets near to 2000, so this is a convenient somewhat middle time-frame. Here we decided to use the world population growth rate (World Bank [33]) which varies by year as shown in Appendix C in Figure C1. We used the average growth rate per ½ decade for iterative projections of about 1.3% (from 2000 to 2019) to 1.8% (from 2000 down to 1955) per year.

To justify this projection, we see that Figure A2a illustrates that building material aggregates (USGS [34]) used to build cities and roads correlates well to population growth (USGS Population Growth [35]).

It is also interesting to note that building materials for cities and roads also correlates well to global warming trends (NASA [36]) shown in Figure A2b.

Column 2 in Table 3 shows the projections with the actual year (~2000) data point tabulated value also listed in the table (see also Table 1). The UHI area amplification factors (Column 3) is then applied to Schneider [20] and GRUMP [21] studies shown in Column 4 using Equation 4.

As an example of the EAA calculation in Table 3, using Eq. 4, the 2019 Schneider 3.1 amplification factor is used as follows:

$$(0.188\text{-}0.59)\ x\ 3.1 + 0.59 = 0.459 \tag{5}$$

Table 3. Extrapolated and amplified urbanized coverage estimates

Year	Urban coverage percent of Earth	Amplification factor	Effective Amplified Area (EAA)
Schneider study [20]			
1950	0.059*	1	**0.059%**
2000-2001	0.0051x29%=0.148		
2019	0.188*	3.1 AF_{Area}**	**0.459%**
2019	0.188*	8.4 AF_{Dome}**	**1.143%**
Worst-case GRUMP study [21]			
1950	0.316%*	1	**0.316%**
2000	0.027x29%=0.783%		
2019	0.952%*	3.1 AF_{UHI}**	**2.288%**
2019	0.952%*	8.4 AF_{Dome}**	**5.658%**

*Growth rate of cities using world population yearly growth rate in Fig A1, **AF_{UHI} is the area amplification factor for 2019 referenced to 1950.

2.5 Weighted Amplification Albedo Solar Urbanization (WAASU) Model Overview

The WAASU model is very straightforward; the weighted model is rigorously derived in Appendix A and is based on a global weighted albedo model. The weighted solar albedo model for 1950 is

$$\alpha_{1950} = \frac{0.33}{A_E}\sum \hat{A}_i \alpha_i + \frac{0.33}{A_E} A_{UHI}\ \alpha_{UHI} + \frac{A_C}{A_E}\alpha_C \tag{6}$$

and for 2019 the WAASU model is

$$\alpha_{2019} = \frac{0.33}{A_E'}\sum \hat{A}_i \alpha_i + \frac{0.33}{A_E'} A_{UHI}\, AF_{UHI}\, \alpha_{UHI} + \frac{A_C}{A_E'}\alpha_C \tag{7}$$

Here α is the Earth's Albedo, α_i is the albedo of each Earth component with the associated surface area $\hat{A}_i$ (the hat indicating all areas excluding the UHI area), similarly α_{UHI} is the UHI albedo associated with its area A_{UHI}, AF is the UHI amplification factor (Sec. 2.1 and 2.2) and A_C is the cloud coverage area with average cloud albedo α_C (Appendix E). As explained in Appendix A, the 0.33 factor arises from the fact that 67% of the Earth is approximately covered by clouds [37].

As well, A_E Earth's surface area in 1950 and A_E' is the Earth's area in 2019 due to the EAA_{UHI} effective solar area increase, is given by

$$A_E' = \hat{A}_E + EAA_{UHI} \tag{8}$$

Here EAA is defined in Eq. 4. Therefore, this increase requires renormalization that is discussed in Section 2.5.1. For example, if water covers 56% of the Earth, now it will be slightly less since the Earth's solar area has increased due to the buildup of cities since 1950 from the number of tall buildings that have increased the Earth's solar surface area along with other UHI amplification effects. This is captured in the solar effective amplified area.

It is important to note in the WAASU model (Eq. 7) that AF is combined with the UHI area and its albedo value

$$(A_{UHI})\,(AF_{UHI})\,(\alpha_{UHI}) \tag{9}$$

This shows the combined effect of the factor in the model and its possible influence on each factor. However, an assumption of the model is α_{UHI}=0.12 and stays generally constant from 1950 to 2019. Average UHI albedo does not appear to vary much over time in the literature [38]. Therefore, consistent with Eq. 9 we find the amplification effect is mainly related to area growth as described in Sec. 2.1. This allows us to use the term as an effective amplified area (EAA) for the part A_{UHI} x A.

Note that all the effective surface areas are influenced by the solar irradiance

$$Effective\,Surface Area = Surface\,Area\,x\,\%Solar\,Irradiance. \tag{10}$$

where the surface area includes all areas including EAA. However, we note that the change in the Earth Albedo over time (from 1950 to 2019), is just a function of the UHI area variation, (when holding all unrelated UHI components constant), that is

$$\left(\frac{d\alpha}{dt}\right)_{EA'} \approx \sum\left(Albedo_{UHI}\,x\,\%Solar\,Irradiance\,x\,\frac{dSurfaceArea_{UHI}}{dt}\right)_i, \tag{11}$$

Here EA' is all other Earth components (held constant). That is the main effect is the UHI surface area change from 1950 to 2019, the albedo and solar irradiance are considered constant.

2.5.1 Model Constraints

Because of Eq. 8, this model is subject to the constraint

$$Total\,Area = \sum_i \{\%\,Normalized\,Effective\,Amplified\,SurfaceAreas_i\} + \%Cloud\,Area = 100\% \tag{12}$$

the small change in area EAA_{UHI} will increase A_E slightly as described by Eq. 8. This requires renormalization to meet the requirements of Eq. 12. All areas change slightly including EAA_{UHI}. The UHI change is termed the normalization effective amplified area (NEAA). A full renormalization example is provided in Appendix F.

To simplify things as much as possible, ***only five Earth constituents are used:*** *water, sea ice, land, UHI coverage, and clouds* (where *land* is its area minus the UHI coverage). These components are fairly easy to estimate and references for their values are provided in Appendix E. Furthermore, we use consistent values found in the IPCC AR5 report (Hartmann et al. [8]) assessment of the Earth's energy budget for solar irradiance. Table 4 summarizes the constraints from these IPCC values.

Table 4. IPCC Earth energy budget values (Hartmann et al. [8])

IPCC Item 2013 Budget	**Incident and Reflected Radiation (W/m^2)**	**Albedo % α**	P_α* **Absorbed (W/m^2)**
Earth	100/340	**29.412**	240=340x(1-.294)
Atmosphere & Clouds	76/340	**22.353**	**79**
Earth Surface Albedo	24/340	**7.059**	**161**
Year	**GHG Effect***	**Surface T(^{o}K)***	**Power**
1950 No GHG Effect	P_α x 1	**255 (-18.09^{o}C)**	**240**
1950 With GHG Effect	P_α x **1.62***	**287.3 (14.6^{o}C)**	**388.8 (=240x1.62)**

*1.62≈β^4, effective emissivity of the planetary system (average GHG re-radiation factor), P_α=340W/m^2(1-α), and T=$(P/\sigma)^{0.25}$

The fixed components of our model maintain relative consistency from 1950 to 2019. The non-fixed value is the urban coverage as indicated by Equation 11. The only unknown value is the *land* albedo (minus the UHI coverage) and this value is adjusted to obtain the IPCC global albedo, 29.412%, and its Earth surface value of incident/reflected value of 7.059 (see Table 5a).

These values are used as a 1950 starting point and then the 2019 increase for the UHI coverage area is inserted. This increases the Earth's area to greater than 100%. Therefore, renormalization is done per the constraint of Equation 12. Renormalization is detailed in Appendix F.

3 Results

Using the extrapolated area coverage in Table 3 with the 3.1 amplification factor applied to the urbanized growth, the resulting global albedo change occurred of 29.399% in 2019 (Table 5b) compared to the earlier 1950 albedo value of 29.412% (Table 5a) for the Schneider nominal case. As well, for the GRUMP worst-case, the albedo changed from 29.412% (Table 6a) to 29.352% (Table 6b) due to the urbanized growth**.** Dome global albedo values are also provided in Appendix F.

As we mentioned earlier, the increases in the solar surface area of the Earth, which will occur with city growth of tall buildings and their solar areas, however comparatively small, requires renormalization of the Earth's surface components in the WAASU model (detailed in Appendix F). This information is displayed in Column 3 in Tables 5b and 6b. While the model is sensitive to urban coverage changes, it works well with renormalization showing a high level of consistency to urban coverage proportionality changes. This consistency is indicated in Table 7 where we find the GRUMP and Schneider long wavelength radiation (LWR) forcing per %EAA averages about 0.096% (W/m^2)/%NEAA in the last column.

Table 5a. Schneider 1950 effective estimate

Surface	Albedo	%NEAA	Cloud Effect %NEAA	Weighted Albedo %
	A	B	C= B x (1-0.67)	A x C
Sum of Water Type		71		
Sea Ice	0.6	15	4.95	2.970
Water	0.06	56	18.48	1.109
Sum of Land Type		29		
Land - (UHI + Coverage)	0.312	28.941	9.551	2.978
UHI + Coverage	0.12	0.059	0.02	0.002
		∑=100.000	33.000	7.059
			Cloud Area	
Clouds	0.334	67	67	22.353
∑ Sum Earth %			100.000	
∑ Global Albedo				29.412

Table 5b. Schneider 2019 effective estimate (AF=3.1)

Surface	Albedo	%NEAA	Cloud Effect %NEAA	Weighted Albedo %
	A	B	C= B x (1-0.67)	A x C
Sum of Water Type		70.717		
Sea Ice	0.6	14.94	4.930	2.958
Water	0.06	55.777	18.406	1.104
Sum of Land Type		29.283		
Land - (UHI + Coverage)	0.312	28.826	9.513	2.966
UHI + Coverage	0.12	0.4571	0.151	0.018
		∑=100.000	33.00	7.028
			Cloud Area	
Clouds	0.334	67	67	22.353
∑ Sum Earth %			100.000	
∑ Global Albedo				29.399

Table 6a. GRUMP 1950 effective estimate

Surface	Albedo	%NEAA	Cloud Effect %NEAA	Weighted Albedo %
	A	B	C= B x (1-0.67)	A x C
Sum of Water Type		71		
Sea Ice	0.6	15	4.95	2.970
Water	0.06	56	18.48	1.109
Sum of Land Type		29		
Land - (UHI + Coverage)	0.314	28.684	9.466	2.968
UHI + Coverage	0.12	0.316	0.104	0.013
		∑=100.000	33.000	7.059
			Cloud Area	
Clouds	0.334	67	67	22.353
∑ Sum Earth %			100.000	
∑ Global Albedo				29.412

Table 6b. Grump 2019effective estimate (AF=3.1)

Surface	Albedo	%EAA	Cloud Effect %NEAA	Weighted Albedo %
	A	B	C= B x (1-0.67)	A x C
Sum of Water Type		69.627		
Sea Ice	0.6	14.71	4.854	2.913
Water	0.06	54.917	18.123	1.087
Sum of Land Type		30.373		
Land - (UHI + Coverage)	0.314	28.129	9.283	2.910
UHI + Coverage	0.12	2.244	0.740	0.089
		∑=100.000	33.000	6.910
			Cloud Area	
Clouds	0.334	67	67	22.353
∑ Sum Earth %			100.000	
∑ Global Albedo				29.352

Table 7 provides a summary of albedo changes found in the WASSU model along with the expected solar longwave radiation increase. From the above global WAASU model, the estimates of the Earth's LWR emissions are obtained from the fundamental expression

$$P_\alpha = 340 \text{ W/m}^2 \text{ (1-Albedo)}. \quad (13)$$

Then the albedo change from 1950 to 2019 represents the equivalent increase in LWR is given by

$$\Delta P_{\alpha} = 340 \text{ W/m}^2 \{(1\text{-Albedo})_{2019} - (1\text{-Albedo})_{1950}\}. \quad (14)$$

The results are compiled in Table 7. The table also includes "What if" estimates, if we could change urbanization to be more reflective with cool roofs to reverse the effect.

Table 7. Albedo and radiative increase model results with UHI effective area.

Year	UHI Area %	UHI %EAA AF=3.1 AF=8.4	UHI NEAA Global Surface %Area	Albedo Cities	Global Weighted Albedo %	Forcing LWR* ΔP_{α} UHI W/m^2	$\frac{\Delta P_{\alpha}\ (W/m^2)}{\%NEAA}$ $\left(\frac{\Delta P_{\alpha}\ (W/m^2)}{\%Albedo}\right)$
Nominal Case Schneider Study							
1950	0.059	0.059	0.059	0.12	29.412	0	—
2019	0.188	0.459	0.457	0.12	29.399	0.044	0.096 (1.0)
2019	0.188	1.143	1.131	0.12	29.379	0.112	0.10 (1.0)
What if	0.188 0.188	0.459 1.58	0.457 1.13	0.202 0.209	29.412	-0.042 -1.129	—
Worst-Case GRUMP Study							
1950	0.316	0.316	0.316	0.12	29.412	0	—
2019	0.952	2.288	2.243	0.12	29.352	0.204	0.091 (1.0)
2019	0.952	5.658	5.395	0.12	29.255	0.534	0.099 (1.0)
What if	0.952 0.952	2.288 5.658	2.244 5.395	0.201 0.209	29.412	-0.204 -0.537	—

*LWR Forcing values do not include the additional GHG re-radiation (see Table 8).

The overall results are summarized:

- Schneider nominal case from 1950 to 2019, the increase in LWR forcing (Row 7) is 0.042W/m^2 and 0.11W/m^2 due to urban area and dome amplification coverage respectively. These values do not include the addition of GHG re-radiation (see Table 8).
- GRUMP worst-case from 1950 to 2019 the increase in LWR (Row 7) is 0.204W/m^2 and 0.537W/m^2 due to urban area and dome amplification coverage respectively. These values do not include the addition of GHG re-radiation (see Table 8).
- The forcing per unit %NEAA or %EAA has consistency with small variability and averaging about 0.096 *W/m^2/%NEAA*. We also note in Column 8 the consistent value of 1.0 W/m^2/%Δalbedo. This is the percent change from the initial albedo value of 29.413% This value is a useful constant and can be derived [39]. Note these values do not include GHG re-radiation (see Sec. 4).
- "What if" corrective action results of cool roofs indicate that changing city albedos in both the Schneider and the GRUMP case from 0.12 to an average value of 0.205 would reverse the increase forcing back to 1950 levels. By comparison, He et al. [40] found the average albedo varies from 0.1 to 0.4, averaging 0.25. Note our model found the average land albedo slightly higher at 0.31 (Table 5 and 6).

4. Discussion on the Relative Contribution to Global Warming Forcing due to UHIs

In this section, the LWR results in Table 7 are adjusted by including GHG re-radiation forcing that will additionally occur. As well, the total global warming forcing contributions are described.

4.1 Full UHI radiation forcing and associated temperature rise

Estimates in Table 7 provide the LWR forcing, but the anticipated average GHG additional re-radiation forcing increase expected is not included. This average re-radiation GHG factor is roughly estimated as 1.62 [39] (this 62% factor is approximately equal to β^4, the effective emissivity of the planetary system) and is exemplified in Table 4. Table 8, Column 4 provides the forcing when the 1.62 factor GHG re-radiation is included and Column 5 shows the associated temperature increase. Appendix G provides an overview of these estimates.

4.2 IPCC/NOAA Radiation Forcing Comparison

To make relative comparisons with UHI forcing, we compare the forcing results in Table 8 to the IPCC estimate for GHG forcing from the period 1950 to 2019, and GHG warming associated temperature rise. The GHG forcing estimate by IPCC/NOAA [41] is 2.38 W/m^2 during this period.

One should note that this value does not include "feedback" (i.e., arctic snow and ice melting) as "forcing" is our primary concern. Column 6 in Table 8 shows the relative forcing ratio to compare it to the UHI strength. For example, the LWR found in the Schneider case for the albedo of 29.3994 was 0.044 W/m^2 in Table 7. Then we estimate with GHG re-radiation as 0.044 W/m^2 X 1.62=0.071 W/m^2 in Column 4 and relative to the IPCC GHG forcing estimate is about 3% (=0.071/2.38) in Column 6, Table 8. One can also obtain the same percentages in Column 6 by dividing the temperature increase in Column 5 by 0.44^{o}C. Here 0.44^{o}C is the temperature rise one obtains from IPCC/NOAA 2.38W/m^2 of forcing without feedback (see Appendix G).

Table 8. WAASU Model full forcing and global warming estimate due to UHI in 2019

UHI EAA Global Surface %Area	Global Weighted Albedo	Percent Albedo Change from 29.412	Full UHI Forcing P_α Includes GHG Re-Radiation LWRx1.62 W/m^2	UHI Temperature ΔT_{UHI} (^{o}C)	UHI GW Percent Relative to IPCC/NOAA GHG Forcing of 2.38 W/m^2
Schneider Case					
0.459	29.399	0.044%	0.071	0.013	3%
1.143	29.379	0.11%	0.182	0.034	7.6%
GRUMP Case					
2.288	29.352	0.2%	0.33	0.061	13.8%
5.658	29.255	0.53	0.865	0.16	36.3%

Finally, the forcing estimate in Column 8, Table 7 is updated in Table 8 from Column 4 divided by Column 3 as

$$\alpha_{Global\_Forcing} = 1.62\,x\,1.0 W/m^2/\%\Delta Albedo = 1.62 W/m^2/\%\Delta Albedo \quad (15)$$

and from Table 8, Column 4 divided by Column 1, the consistent forcing per %EAA estimate is

$$UHI_{AAA\_Forcing} \approx 1.62\,x\,0.096 W/m^2/\%EAA = 0.16 W/m^2/\%EAA \quad (16)$$

Examples of how these might be used are provided in Appendix G. Lastly, as a check, one may note that UHI global warming estimates roughly scale with UHI size as might be expected. For example, in Table 1 the ratio of Schneider to Grump UHI area extent is 2.7/0.51=5.3. We note the values in the last column in Table 8 scale close to this factor (i.e. 3% x 5.3=15.9% which is close to 13.8% and 7.6% x 5.3=40% close to 36%) between Schneider and GRUMP, respectively.

5. Conclusions

In this paper, we derived a versatile WAASU model and applied it to provide estimates of the UHI effect (with urban areas) on global warming. This calculation was done with the aid of assumptions for UHI solar amplification factors. These estimates inserted into our WAASU model found that between 0.071W/m^2 to 0.87W/m^2 of radiative forcing (Table 8) may be possible. This forcing result indicates that about 3% to 36% of global warming may be due to the UHI effect by comparisons to anticipated GHG forcing (when feedback temperature increases are not included). However in terms of related climate feedback warming, some authors have suggested a factor of two [27-29] for water-vapor. Additionally, in Appendix D, we found using a WAS model about a 0.15^{o}C rise due to ice loss. This represents about 16% of GW in 2019. Thus, including these two positive feedbacks, our UHI results could possibly be almost a factor of 3 times higher in terms of potential influence on the total amount of GW. The wide variations in our forcing estimates are due to both the amplification and urban area uncertainties. However, the model found that the forcing per effective amplified UHI area and albedo estimates were consistent showing 0.16W/m^2/%EAA and 1.62 W/m^2/%Δalbedo, respectively (see Eq. 15 and 16). In terms of human land use contamination contributions to global warming, these results are possibly conservative due to the limitations of the

WAASU model that cannot include rural human habitation, rural roads and rooftops, deforestation, draught related fires, associated evapotranspiration loss, and so forth.

However, the WAASU model is versatile. We are able to quickly estimate UHI albedo changes required to offset the estimated forcing. For example, "What if" corrective action results of cool roofs indicated that an average UHI albedos change from 0.12 to an average value of 0.21 would reverse the UHI forcing back to 1950 levels. This value was found to be close to the average global land surface albedo of 0.25 [40].

Therefore the model can provide albedo-area estimates for reverse forcing similar to the "What if" corrective actions for mitigation/adaptation strategies. As a follow-up study, the author has proposed a similar modeling strategy to estimate select areas and albedo changes necessary for surface albedo type global warming solutions [39].

Another example of the model's versatility was demonstrated by using the weighted albedo solar model for estimating the temperature rise due to ice loss in Appendix D.

Below, we provide suggestions and corrective actions, which include:

- Albedo guidelines for both UHIs and roads similar to ongoing CO_2 efforts
- Adding albedo controls to the Paris Climate Accord
- Guidelines for future albedo design considerations of cities.
- Recommend an agency like NASA to be tasked with finding applicable solutions to cool UHIs.
- Recommend cars to be more reflective. Although world-wide vehicles likely do not embody much of the Earth's area, recommending that all newly manufactured cars to be higher in reflectivity (e.g., silver or white) would help raise awareness of this issue similar to electric automobiles that help improve CO2 emissions.

Appendix A: Derivation of the WASSU Model

The Earth's long-wavelength radiation power P in W/m^2 is given by

$$P = \frac{S_o}{4}(1-\alpha) \tag{A-1}$$

Here α is the Earth's albedo and S_o=1360 W/m^2. From Equation A-1, the albedo can be written

$$\alpha = 1 - \frac{4P}{S_o} \tag{A-2}$$

Let small p indicate the power in watts so that

$$p(watts) = A_E \; P(W/m^2) \tag{A-3}$$

This is useful for re-writing Eq. A-1 in terms of the Earth's areas A_E for surface land area A_S and cloud coverage area A_C, receiving solar power. This gives

$$p(watts) = A_E \frac{S_o}{4}(1-\alpha) = (A_S + A_C)\frac{S_o}{4}(1-\alpha) = (0.33A_E + A_C)\frac{S_o}{4}(1-\alpha) \tag{A-4}$$

Here it is assumed that on average 33% of the Earth receives direct sunlight or 67% is covered by clouds [Ref. 37, Appendix E], that is the Earth's primary solar area is

$$A_E = A_S + A_C = 0.33A_E + A_C \tag{A-5}$$

Now we can divide Eq. A-4 through by A_E and the $S_o/4$ term and expand out the Earth's areas as

$$\frac{4p}{A_E S_o} = \frac{4P}{S_o} = \frac{(0.33A_E + A_C)}{A_E}(1-\alpha) = \frac{0.33}{A_E}\sum A_i\,(1-\alpha_i) + \frac{A_C}{A_E}(1-\alpha_C) \tag{A-6}$$

Here Ai and Ac are surface area and cloud area coverages, while α_i and α_c are their associated albedo values. Then expanding terms on the RHS we have

$$\frac{4P}{S_o} = \frac{0.33}{A_E}\sum A_i - \frac{0.33}{A_E}\sum A_i\alpha_i + \frac{A_C}{A_E} - \frac{A_C}{A_E}\alpha_C \tag{A-7}$$

Collecting terms we can write

$$\frac{4P}{S_o} = \left\{\frac{0.33}{A_E}\sum A_i + \frac{A_C}{A_E}\right\} - \frac{0.33}{A_E}\sum A_i\,\alpha_i - \frac{A_C}{A_E}\alpha_C \tag{A-8}$$

Note that in Eq. A-8 the first term on the RHS is unity

$$\left\{\frac{0.33}{A_E}\sum A_i + \frac{A_C}{A_E}\right\} = \frac{A_S + A_C}{A_E} = 1 \tag{A-9}$$

Then Eq. A-8 is now

$$\frac{4P}{S_o} = 1 - (\frac{0.33}{A_E}\sum A_i\alpha_i + \frac{A_C}{A_E}\alpha_C) \tag{A-10}$$

or

$$1 - \frac{4P}{S_o} = \frac{0.33}{A_E}\sum A_i\,\alpha_i + \frac{A_C}{A_E}\alpha_C \tag{A-11}$$

Combining this with Eq. A-2, the Weighted Albedo Solar (WAS) model is

$$\alpha = \frac{0.33}{A_E}\sum A_i\alpha_i + \frac{A_C}{A_E}\alpha_C \tag{A-12}$$

However, further weighting the model with the UHI amplification factor AF_{UHI} by expanding out A_i to treat the UHI area separately yields our final Weighted Amplification Solar Urbanization (WAASU) model

$$\alpha = \frac{0.33}{A_E}\sum \hat{A}_i\alpha_i + \frac{0.33}{A_E}A_{UHI}\,AF_{UHI}\,\alpha_{UHI} + \frac{A_C}{A_E}\alpha_C \tag{A-13}$$

The inclusion of AF_{UHI} is presented as a weighting factor in the only logical part of the equation for the WAASU model. Here, the first term $\hat{A}_i$ with the hat indicates all surface areas of the Earth except the UHI area, and the 2nd term is broken out for the UHI sum to include the AF term. We note that AF_{UHI_1950}=1 and AF_{UHI_2019}>1 (see Sec. 2.1 and 2.2 for this factor). Note that we take α_{UHI}=0.12 [42] as constant from 1950 to 2019, then A_{UHI} x AF_{UHI} can be considered as an effective area amplification factor. The α_{UHI}=0.12 [42] appears somewhat on the low end for average UHI albedos from some studies [38]. However, in general, albedo reporting appears somewhat constant in time over city growth [38].

Appendix B: UHI Dominant Amplification Effects and Climate Effects

The UHI amplification effects that we consider to dominate listed in Table 2 are as follows:

- ***The heat capacity and solar heating area amplification effect:*** Solar surface areas of buildings make the city much larger than its actual surface area in terms of solar absorption. Thus, solar building area amplification may be the most dominant aspect of the UHI climate area. When this is included with the massive heat capacities of building, the combined effect creates a day-night heat cycle. In most cities, it is observed that daytime atmospheric temperatures are cooler compared to night. For example, in a study by Basara et al. [43] in Oklahoma city UHI, it was found that at just 9-m height, the UHI was consistently 0.5–1.75°C greater in the urban core than the surrounding rural locations at night. Further, in general, the UHI impact was strongest during the overnight hours and weakest during the day. This inversion effect can be the result of massive UHI buildings acting like heat sinks, having giant heat capacities, and storing heat in their reservoir via convection as solar radiation is absorbed during the day. This occurrence often reduces the UHI day effect, but at night buildings cool down, giving off their stored heat that increases local temperatures to the surrounding atmosphere. This effect increases with city growth as buildings have gotten substantially taller since 1950 (Barr [44]).

- ***The hydro-hotspot amplification effect:*** This effect is not well addressed in the literature. Atmospheric moisture source is a complex issue due to Hydro-HotSpots (HHS). HHS occurs when buildings are hot due to sun exposure. Then, during precipitation periods, the hot evaporation surfaces increase localized water vapor as warm air holds more moisture. This increase likely acts at times as a local greenhouse gas that blankets city heat and increases infrared radiation during these periods, providing another UHI humidity amplification source. This effect combined with the heat storage occurring from daytime hours indicates that the effect may occur even during nighttime precipitation. The level of hydro-hotspot significance in climate change is currently unknown. However, observations of this effect are reasonably well established in observed humidity effects.

  The humidity amplification effect: This effect has been observed. For example, Zhao et al. [45] noted that UHI temperature increases in daytime ΔT by 3.0°C in humid climates but decreasing ΔT by 1.5°C in dry climates. They noted that such relationships imply UHIs will exacerbate heat wave stress on human health in wet UHI climates. They found a strong correlation between ΔT increase and daytime precipitation. Their results concluded that albedo management would be a viable means of reducing ΔT on large scales.

- ***Reduced wind cooling and solar canyons:*** In UHIs reduced wind is a known effect due to building wind friction that inhibits cooling by convection. Tall buildings also create solar canyons and trap sunlight, reducing the average albedo, although some benefits occur from shading. In general, both have the effect of amplifying the temperature profile of UHIs.

Many of these amplification effects create local and global climate issues for over 50% of the world population that now lives in cities. We summarize theses climate issues as follows:

- UHIs are warmer than their rural vicinities and create a dome of warmer air above cities
- Wind reduction due to building resistance create cooling losses
- Often city rainfall rates are noticeably higher. Common hypotheses include the fact that warm air creates turbulence and pollution supplies extra nuclei that encourage cloud rain droplets
- Increases in the evaporation rate from hot impermeable surfaces during precipitation (hydro-hotspots) can increase atmospheric GHG water vapor contributing to a local temperature increase (see next bullet).
- UHI temperatures increase in daytime ΔT by 3.0°C in humid climates but decrease ΔT by 1.5°C in dry climates [45]. A strong correlation has been found between ΔT increase and daytime precipitation. Their results concluded that albedo management would be a viable means of reducing ΔT on large scales.
- This humidity effect may extend the daytime issue into nighttime depending on a city's heat capacity
- Because of the increase in air pollutants, including CO_2 from automobiles, there is an increase in the GHG warming effect as compared to non-urban areas
- Reduction of natural vegetation in UHIs lessens the possibilities for the evapotranspiration process and thereby reduces the natural cooling effect since vegetation is scarce
- The UHI footprint increases evapotranspiration losses into the nearby rural areas and the cities heat capacity increase the length of time these losses occur
- Impervious surfaces add to the loss of evapotranspiration with incease water runoff compared to rural areas
- Increases in the evaporation rate also create warmer ground temperatures over longer periods creating dryness and including local forest that can be prone to fires
- Anthropogenic heating creates some surface temperatures increases, also amplifying the UHI effect.

- The accumulation of these effects increases the manmade UHI thermal forcing mechanism that adds to global warming and potentially can escalate the feedback climate inertia warming problems as well.

Appendix C: Growth Rates and Information on Natural Aggregates

Below is a plot of the world population growth rate that varies from about 2.1% to 1.1%. This graph is used to make growth rate estimates of urban coverage. We note that natural aggregates used to build cities and roads are reasonably correlated to population growth in Figure C2a. Also of interest (Fig. C2b) is the fact that one can see some correlation to global warming with the use of natural aggregates.

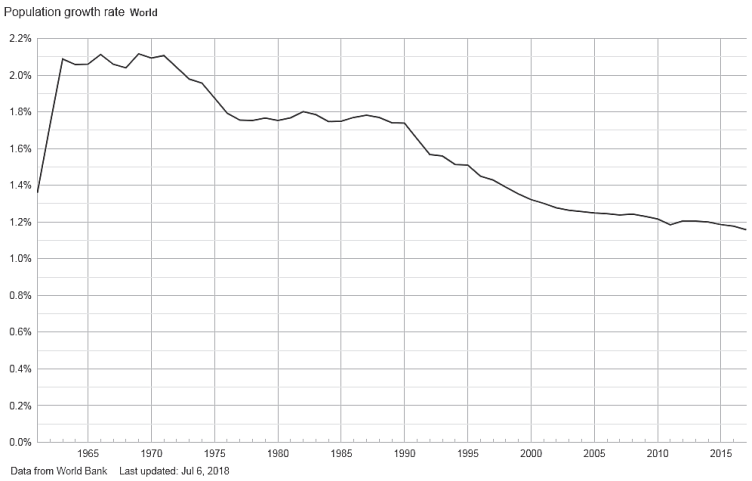

Figure C1. Population growth rate by year from 1960 to 2018, World Bank, [33]

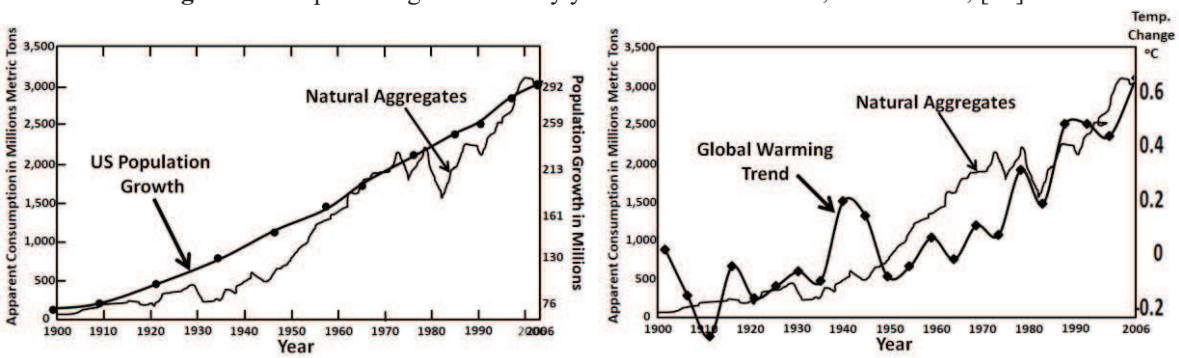

Figure C2. a) Natural aggregates [34] correlated to U.S. Population Growth (USGS [33]) **b)** Natural aggregates [33] correlated to global warming (NASA [36])

Appendix D: *Weighted Albedo Solar Model Applied to the Melting of Sea Ice*

The weighted albedo solar (WAS) model (Eq. A-12) derived in Appendix A can be used to estimate the warming feedback due to sea ice loss in the Arctic. We need to make several initial estimates to obtain a ballpark number of warming due to sea ice loss. The first estimate is that the Antarctic sea ice has remained roughly constant (NOAA, Scott [45] over the last two decades. Next, it is estimated that the Arctic sea ice area is about 60% larger on average compared with Antarctic sea ice areas yearly (NOAA, Scott [45]). It has been observed that the Arctic sea ice is melting at an alarming rate of 12.85% per decade in the last two decades (NASA sea ice [47]). This apparent trend appears to yield an estimated 26% decrease in sea ice in the last two decades. It is difficult to find a strong reference for quantifying global warming impact due to Arctic sea ice melting. However, we can get an approximation from the WAS model (and further illustrate the strengths of these models). Sea ice melting will result in a significant albedo change that roughly changes the ice-albedo of 0.6, to the open ocean albedo of 0.06 (see Table D1 and D2). Fortunately, the Arctic areas receive only about 40% as much solar radiation (Sciencing [50]) reducing the feedback effect. From Equation 10, the effective sea ice surface area reduction from the irradiance decrease can be approximated as

$$\text{Effective Arctic Sea Ice Surface Area} = 0.6 \times 15\% \{1-(0.257 \times 0.40)\} = 8.064\% \quad \text{(D-1)}$$

Here 0.6 x 15% is sea ice percent in the Arctic area, 0.26 is the fraction of sea ice lost, and 40% is the solar irradiance effect. Then adding the Antarctic average sea ice area, the total sea ice area is reduced from 15% to

$$\text{Sea Ice area 2019} = 0.4x15\% + 8.064 = 14.06\% \quad \text{(D-2)}$$

This is a 0.94% decrease from 15%. In the WAS model, we will have to assume that the effective ocean surface area increases proportionately by 0.94% to 56.94% (see Table D2). The WAS model then finds that the global albedo change decreases from 29.412% to 29.244%. (Note that alternately we could have set the albedo to 29.412% in 2019 and worked back to 1950. In this case, the albedo would have increased to 29.244%).

The percent Global Warming (GW) is found as:

$$\%GW = \{(P/\sigma)^{0.25}_{2019} - (P/\sigma)^{0.25}_{1950}\}/0.95^{o}C, \quad \text{(D-3)}$$

where $P=340W/m^2$ x (1-Albedo). The warming increase due to ice melting is estimated from this model to be about $0.15^{o}C$ or 15.8% when compared to a warming trend of $0.95^{o}C$ increase in 2019. The increase in radiative forcing is 0.6 W/m^2. The feedback is then roughly 0.63 $W/m^2/^{o}K$ where we assume a temperature change of $0.95^{o}C$.

These values should only be taken as a rough estimate due to numerous uncertainties as climatologists find it hard to fully quantify the seasonal variations in ice change and to know the possible impact on cloud coverage increase from additional warming evaporation. However, one would expect less evaporation in the Arctic. Thus, there are a lot of uncertainties.

Table D1. Baseline (Albedo=29.412, 1950)

Surface	Albedo	%Area	Cloud Effect %NEAA	Weighted Albedo %
	A	B	C= B x (1-0.67)	A x C
Sum of Water Type		71		
Sea Ice	0.6	15	4.95	2.970
Water	0.06	56	18.48	1.109
155Sum of Land Type		29		
Land - (UHI + Coverage)	0.312	28.941	9.551	2.978
UHI + Coverage	0.12	0.059	0.02	0.002
		∑=100.000	33.000	7.059
			Cloud Area	
Clouds	0.334	67	67	22.353
∑ Sum Earth %			100.000	
∑ Global Albedo				29.412

Table D2. Sea ice loss - albedo change (29.2443%, 2019)

Surface	Albedo	%NArea	Cloud Effect %NEAA	Weighted Albedo %
	A	B	C= B x (1-0.67)	A x C
Sum of Water Type		71		
Sea Ice	0.6	14.06	4.435	2.507
Water	0.06	56.94	18.995	1.14
Sum of Land Type		29	23.43	
Land - (UHI + Coverage)	0.312	28.941	9.551	2.978
UHI + Coverage	0.12	0.059	0.02	0.002
		100.000	33.000	6.64
			Cloud Area	
Clouds	0.334	67	67	22.353
∑ Sum Earth %			123.430	
∑ Global Albedo				29.244

Appendix E: WAASU Model References

Table E1 provides references for the WAASU model values.

Table E1 Key References for WAASU model

Parameter	Albedo References	1950 Area References
Sea Ice	50-70%, average 60% (NSID [51])	15% (Lindsey [52])
Water	6% (NSID [51])	56% Ocean+Sea Ice=71% (USGS [53])
Land-(UHI+Coverage)	Adjusted to obtain 29.412% and surface reflected of 7.06 Earth Albedo in 1950 thereafter held fixed (see IPCC Hartmann [8] AR5 report)	29%-Urban Coverage
Avg. UHI+Cov	0.12 Sugawara et. Al [42], 0.15 Tricia, A [38]	See Table 1
Clouds	22.353 (IPCC Hartmann et al. [8])	67% (Earthobservatory, NASA [54])
Earth Albedo	29.412% (IPCC Hartmann [8])	-

Appendix F: Albedo Model Renormalization Information

Table F1 is reproduced from above, while Table F2 is the results of the Schneider dome area case. The results are used to demonstrate how normalization is performed

Table F1. Schneider 1950 estimates

Surface	Albedo	%NEAA	Cloud Effect %NEAA	Weighted Albedo %
	A	B	C= B x (1-0.67)	A x C
Sum of Water Type		71		
Sea Ice	0.6	15	4.95	2.970
Water	0.06	56	18.48	1.109
Sum of Land Type		29		
Land - (UHI + Coverage)	0.312	28.941	9.551	2.978
UHI + Coverage	0.12	0.059	0.02	0.002
		∑=100.000	33.000	7.059
			Cloud Area	
Clouds	0.334	67	67	22.353
∑ Sum Earth %			100.000	
∑ Global Albedo				29.412

Table F2. Schneider 2019 Dome estimate (AF=8.4)

Surface	Albedo	%NEAA	Cloud Effect %NEAA	Weighted Albedo %
	A	B	C= B x (1-0.67)	A x C
Sum of Water Type		70.239		
Sea Ice	0.6	14.839	4.897	2.938
Water	0.06	55.4	18.282	1.097
Sum of Land Type		29.761		
Land - (UHI + Coverage)	0.312	28.631	9.448	2.946
UHI + Coverage	0.12	1.1307	0.373	0.045
		∑=100.000	33.000	6.981
			Cloud Area	
Clouds	0.334	67	67	22.353
∑ Sum Earth %			100.000	
∑ Global Albedo				29.379

Normalization is done as follows:

1. The model starts with 1950 Table F1 albedo 29.412%, then the 2019 urban coverage area is entered.
2. For example, in Table F1, Column B the UHI area increases from **0.059%** to 1.143% (not shown) and normalized to **1.131**%. This value is 1.084% larger (=1.143-0.059), now the 'Sum of % of Earth Area' is increased from 100% to 101.084% in 2019.
3. All areas need to be renormalized to 101.084%. For example, sea ice at 15% in 1950 becomes 15%x(100.000/101.084)= **14.839%** and the Urban Coverage becomes 1.143%x(100/101.084)=**1.1307%.**

We also include in this appendix the GRUMP dome estimates. Table F3 is reproduced from above, while Table F4 is the results of the GRUMP dome area case.

Table F3. GRUMP Area 1950 estimates

Surface	Albedo	%NEAA	Cloud Effect %NEAA	Weighted Albedo %
	A	B	C= B x (1-0.67)	A x C
Sum of Water Type		71		
Sea Ice	0.6	15	4.95	2.970
Water	0.06	56	18.48	1.109
Sum of Land Type		29		
Land - (UHI + Coverage)	0.314	28.684	9.466	2.968
UHI + Coverage	0.12	0.316	0.104	0.013
		∑=100.000	33.000	7.059
			Cloud Area	
Clouds	0.333	67	67	22.353
∑ Sum Earth %			100.000	
∑ Global Albedo				29.412

Table F4. GRUMP 2019 dome estimates (AF=8.4)

Surface	Albedo	%NEAA	Cloud Effect %NEAA	Weighted Albedo %
	A	B	C= B x (1-0.67)	A x C
Sum of Water Type		70.239		
Sea Ice	0.6	14.239	4.7	2.82
Water	0.06	53.160	17.54	1.05
Sum of Land Type		29		
Land - (UHI + Coverage)	0.314	27.229	9.0	2.82
UHI + Coverage	0.12	5.371	1.77	0.21
		∑=100.000	33.000	6.9
			Cloud Area	
Clouds	0.334	67	67	22.353
∑ Sum Earth %			100.000	
∑ Global Albedo				29.255

Appendix G: Overview of Estimates in Table 8

The GHG re-radiation effect increases the LWR forcing found in Table 7 by a factor of 1.62 as indicated in Table 4 (see also Feinberg [39]). Then the LWR is modified using this by the standard formula

$$P_{2019} = 340W/m^2 x(1-Albedo_{2019})x1.62 \text{ and } P_{1950} = 340W/m^2 x(1-Albedo_{1950})x1.62 \quad \text{(G-1)}$$

Using this the UHI radiation forcing is

$$\Delta P = P_{2019} - P_{1950} \tag{G-2}$$

Results from this equation are shown in Table 8, Column 4 for each albedo. Next, we obtain a temperature increase. This is given by

$$\Delta T = \{(P_\alpha/\sigma)^{0.25}{}_{2019} - (P_\alpha/\sigma)^{0.25}{}_{1950}\} \tag{G-3}$$

The results are shown in Table 8, Column 5.

IPCC/NOAA Radiation Forcing and Percent Global Warming Comparison

To make comparisons to assess the relative UHI forcing, the above results are referenced to the IPCC estimate for GHG forcing from the period 1950 to 2019, and this associated temperature rise. The GHG forcing estimate by IPCC/NOAA [41] is for this period on GHG forcing is 2.38 W/m^2.

One should note that this value does not include "feedback" (i.e., arctic snow and ice melting) as "forcing" is our primary concern. Column 6 then shows the relative forcing ratio to compare it to the UHI strength. For example, the LWR found in the Schneider case in Table 7 for the albedo of 29.3994 is 0.042 W/m^2. Then we estimate an average of 0.042 W/m^2 X 1.6=0.068 W/m^2 for the full forcing using the GHG re-radiation factor of 1.62. Then relative to the IPCC GHG forcing estimate, this is about 2.9% (=0.068/2.38) shown in Table 8, Column 6.

IPCC/NOAA Global Temperature Rise Due to Forcing Comparison

Next, we estimate the percent of global warming anticipated from the WAASU model results. To do this we need an estimate of the temperature rise due to IPCC/NOAA [41] GHG forcing assessment to make comparisons. Using the albedo of 29.412 for 1950 (Table 7), then the LWR GHG re-radiation energy (using the 1.62 Factor) is

$$P_{\alpha 1950} = 340W/m^2 x(1-.294118)x1.62 = 386.4W/m^2 \tag{G-4}$$

This is converted to the 1950 temperature providing a reasonable estimate of the average global temperature for that year

$$T_{1950} = (386.4W/m^2/\sigma)^{0.25} = 387.31°K \ \ (14.164°C) \tag{G-5}$$

Then the forcing (without feedback) for 2019 according to the IPCC/NOAA [41] value of 2.38W/m2 yields a total radiation of

$$P_{F\alpha 2019} = 386.4W/m^2 + 2.38W/m^2 = 287.78W/m^2 \tag{G-6}$$

This converts to the following temperature

$$T_{F\_2019} = (387.76W/m^2/\sigma)^{0.25} = 387.755°K \ \ (14.605°C) \tag{G-7}$$

This provides a temperature rise of 0.44^{o}C

$$\Delta T_{Forcing} = T_{F\_2019} - T_{1950} = 14.605°C - 14.164°C = 0.44°C \tag{G-8}$$

We note the actual temperature rise with feedback is 0.95^{o}C in 2019. This would require a feedback factor of about 2.15. The factor of 2 has been cited in the literature [27-29] so this is a reasonable estimate. If we consider this to be the actual temperature rise due to all forcing (taken from the IPCC GHG estimate), the relative global warming contribution from the UHI temperature rise is shown in Table 8 in the last column. This is the same as the ratio of GHG forcing. For example, ΔT is 0.013^{o}C for the albedo decrease from 29.4418 to 29.3994% from Eq. 13-15. Then the percent of global warming relative to 0.44^{o}C is 2.9%% (=0.013C/0.44C percent).

Finally, examples for Equation 15 and 16 are provided below:

Example for Eq. 15: Given a global albedo change by 0.2% the forcing expected is

$$\alpha_{Global\_Forcing}=1.6\ 2x\ 1W/m2\ x\ 0.2\%=0.32\ W/m^2\ (Row\ 4) \quad \text{(G-9)}$$

Example for Eq. 16: Given a UHI EAA of 1.14% then the forcing is

$$UHI_{EAA\_Forcing}=1.6\ x\ 0.094W/m^2\ x\ 1.14\%=0.17\ W/m^2\ \text{(Row 3, 0.18 W/m}^2 \quad \text{(G-10)}$$

Conflicts of Interest

The author declares that he has no conflicts of interest.

References

1 McKitrick R. and Michaels J. (2004) A Test of Corrections for Extraneous Signals in Gridded Surface Temperature Data, Climate Research

2 McKitrick R., Michaels P. (2007) Quantifying the influence of anthropogenic surface processes and inhomogeneities on gridded global climate data, J. of Geophysical Research-Atmospheres. Also see McKitrick Website Describing controversy: https://www.rossmckitrick.com/temperature-data-quality.html

3 De Laat, A. T. J., and A. N. Maurellis, (2006) Evidence for the influence of anthropogenic surface processes on lower tropospheric and surface temperature trends. Int. J. Climatol., 26, 897–913

4 IPCC Archive (2007) https://archive.ipcc.ch/publications_and_data/ar4/wg1/en/ch3s3-2-2-2.html

5 Schmidt G. A. (2009) Spurious correlations between recent warming and indices of local economic activity, *Int. J. of Climatology*

6 McKitrick, Ross R. (2010) Atmospheric Oscillations Do Not Explain the Temperature-Industrialization Correlation. *Statistics Politics and Policy* Vol 1. No. 1., July 2010

7 McKitrick, Ross R., and Nicolas Nierenberg (2010) Socioeconomic Patterns in Climate Data. *Journal of Economic and Social Measurement*, 35(3,4) pp. 149-175. DOI 10.3233/JEM-2010-0336.

8 Hartmann, D.L., A.M.G. Klein Tank, M. Rusticucci, L.V. Alexander, S. Brönnimann, Y. Charabi, F.J. Dentener, E.J. Dlugokencky, D.R. Easterling, A. Kaplan, B.J. Soden, P.W. Thorne, M. Wild and P.M. Zhai, 2013: Observations: Atmosphere and Surface. In: Climate Change (2013) The Physical Science Basis. Contribution of Working Group I to the Fifth Assessment Report of the Intergovernmental Panel on Climate Change. Cambridge University Press, Cambridge, United Kingdom and New York, NY, USA.

9 Zhao, Z.-C., (1991) Temperature change in China for the last 39 years and urban effects. Meteorological Monthly (in Chinese), 17(4), 14-17.

10 Feddema, J. J., K. W. Oleson, G. B. Bonan, L. O. Mearns, L. E. Buja, G. A. Meehl, and W. M. Washington (2005), The importance of land-cover change in simulating future climates, *Science*, 310, 1674– 1678, DOI:10.1126/science.1118160

11 Ren, G.-Y., Z.-Y. Chu, J.-X. Zhou, et al., (2008): Urbanization effects on observed surface air temperature in North China. J. Climate, 21, 1333-1348

12 Jones, P. D., D. H. Lister, and Q.-X. Li, (2008) Urbanization effects in large-scale temperature records, with an emphasis on China. J. Geophys. Res., 113, D16122, DOI: 10.1029/2008JD009916.

13 Stone B. (2009) Land use as climate change mitigation, Environ. Sci. Technol., 43(24), 9052– 9056, DOI:10.1021/es902150g

14 Zhao, Z.-C., (2011): Impacts of urbanization on climate change. Earth Science,, Science Press, 843-846.

15 Yang, X.; Hou, Y.; Chen, B. (2011) Observed surface warming induced by urbanization in east China. *J. Geophys. Res. Atmos*, 116, DOI:10.1029/2010JD015452.

16 Huang Q. , Lu Y. (2015) Effect of Urban Heat Island on Climate Warming in the Yangtze River Delta Urban Agglomeration in China, *Intern. J. of Environmental Research and Public Health* 12 (8): 8773

17 Bian, T., Ren, G., Yue, Y. 2017. Effect of urbanization on land-surface temperature at an urban climate station in north China. *Boundary-Layer Meteorology* **165**: 553-567.

18 Conference of the Parties, Adoption of the Paris Agreement, (2015), U.N. Doc. FCCC/CP/2015/L.9/Rev/1

19 Satterthwaite D.E., F. Aragón-Durand, J. Corfee-Morlot, R.B.R. Kiunsi, M. Pelling, D.C. Roberts, and W. Solecki (2014) Urban areas. In: Climate Change Impacts, Adaptation, and Vulnerability. Part A: Global and Sectoral Aspects. Contribution of Working Group II to the Fifth Assessment Report of the Intergovernmental Panel on Climate Change (IPCC)

20 Schneider, A., M. Friedl, and D. Potere, (2009)A new map of global urban extent from MODIS satellite data. Environmental Research Letters, 4(4), 044003, DOI:10.1088/ 1748-9326/4/4/044003

21 Global Rural Urban Mapping Project (GRUMP) (2005), Columbia University Socioeconomic Data and Applications Center, Gridded Population of the World and the Global Rural-Urban Mapping Project (GRUMP).

22 NASA (2000) Gridded population of the world, , https://sedac.ciesin.columbia.edu/data/set/gpw-v3-

population-count/data-download

23 Galka M. (2016) Half the World Lives on 1% of Its Land, Mapped, https://www.citylab.com/equity/2016/01/half-earth-world-population-land-map/422748/, , (2016 publication on 2000 data set, http://metrocosm.com/world-population-split-in-half-map/

24 Zhou Y. , SmithS. , Zhao K., M. Imhoff, A. Thomson, B. Lamberty, G. Asrar, X. Zhang, C. He and C. Elvidge, A global map of urban extent from nightlights, Env. Research Letters, 10 (2015), (2000 data set).

25 Karl, T. R., H. F. Diaz, and G. Kukla (1988), Urbanization: Its detection and effect in the United States climate record, J. Clim., 1, 1099–1123.

26 Chagnon, S. A. (1999), A rare long record of deep soil temperature defines temporal temperature changes and an urban heat island, Clim. Change, 42, 531–538.

27 Manabe, S., and R. T. Wetherald (1967), Thermal equilibrium of the atmosphere with a given distribution of relative humidity, J. Atmos. Sci., 24, 241–259.

28 Randall, D. A.et al. (2007), Climate models and their evaluation, in Climate Change 2007: The Physical Science Basis. Contributions of Working Group I to the Fourth Assessment Report of the Intergovernmental Panel on Climate Change, edited by S. Solomon et al., Cambridge Univ. Press, Cambridge, U.K.

29 Dessler A. E., Zhang Z., Yang P., Water-vapor climate feedback inferred from climate fluctuations, 2003–2008, *Geophysical Research Letters*, (2008), https://doi.org/10.1029/2008GL035333

30 Zhang, X., Friedl, M. A., Schaaf, C. B., Strahler, A. H. & Schneider, A. (2004) The footprint of urban climates on vegetation phenology. *Geophys. Res. Lett. 31, L12209*

31 Zhou D., Zhao S., L. Zhang, G Sun and Y. Liu, (2015), The footprint of urban heat island effect in China, *Scientific Reports*. 5: 11160

32 Fan, Y., Li, Y., Bejan, A. *et al.* Horizontal extent of the urban heat dome flow. *Sci Rep* 7, 11681 (2017). https://doi.org/10.1038/s41598-017-09917-4

33 World Bank (2018) population growth rate, worldbank.org

34 USGS (1900-2006), Materials in Use in U.S. Interstate Highways, https://pubs.usgs.gov/fs/2006/3127/2006-3127.pdf

35 US Population Growth (1900-2006), u-s-history.com/pages/h980.html1

36 NASA, (2020) https://climate.nasa.gov/vital-signs/global-temperature/

37 Earthobservatory, NASA (clouds albedo 0.67) https://earthobservatory.nasa.gov/images/85843/cloudy-earth

38 Tricia, A., Hutyra, L., Schaaf, C., Erb, A.,Wang, J. (2017) Albedo, Land Cover, and Daytime Surface Temperature Variation Across and Urbanized Lanscape, AGU, https://doi.org/10.1002/2017EF000569

39 Feinberg A., (2020) On Geoengineering and Implementing an Albedo Solution with UHI GW and Cooling Estimates vixra 2006.0198, DOI: 10.13140/RG.2.2.26006.37444/6 (Currently in Peer Review in the J. Mitigation and Adaptation Strategies for Global Change)

40 He T, Liang S, and Song DX (2014), Analysis of global land surface albedo climatology and spatial-temporal variation during 1981–2010 from multiple satellite products, J. Geophys. Res. Atmos., 119, 10,281–10,298, DOI:10.1002/ 2014JD021667

41 Butler J., Montzka S., (2020) The NOAA Annual Greenhouse Gas Index, Earth System Research Lab. Global Monitoring Laboratory, https://www.esrl.noaa.gov/gmd/aggi/aggi.html

42 Sugawara, H., Takamura, T. Surface Albedo in Cities (0.12): Case Study in Sapporo and Tokyo, Japan. *Boundary-Layer Meteorol* 153, 539–553 (2014). https://doi.org/10.1007/s10546-014-9952-0

43 Basara J., P. Hall Jr., A.Schroeder, B.Illston, K.Nemunaitis (2008), Diurnal cycle of the Oklahoma City urban heat island, J. of Geophysical Research

44 Barr J. M., (2019) The Economics of Skyscraper Height (Part IV): Construction Costs Around the World, https://buildingtheskyline.org/skyscraper-height-iv/

45 Zhao L, Lee X, Smith RB, Oleson K, Strong (2014), Contributions of local background climate to urban heat islands, Nature. 10;511(7508):216-9. DOI: 10.1038/nature13462

45 NOAA, Scott, M, (2019), Understanding Climate: Antarctic sea ice extent, https://www.climate.gov/print/833949

47 NASA Sea Ice, (2019), https://climate.nasa.gov/vital-signs/arctic-sea-ice/

50 Sciencing (2018) https://sciencing.com/sun-intensity-vs-angle-23529.html

51 NSID (2020), National Snow & Ice Data Center, "Thermodynamics: Albedo". nsidc.org. Retrieved 14 August 2016. https://nsidc.org/cryosphere/seaice/processes/albedo.html

52 Lindsey R, Scott M., (2019), Climate Change: Arctic Sea Ice Summer Minimum, NOAA Climate.gov, https://www.climate.gov/news-features/understanding-climate/climate-change-minimum-arctic-sea-ice-extent

53 USGS on Amount of Earth covered by water, https://www.usgs.gov/special-topic/water-science-school/science/how-much-water-there-earth?qt-science_center_objects=0#qt-science_center_objects

54 Earthobservatory, NASA (clouds albedo 0.67) https://earthobservatory.nasa.gov/images/85843/cloudy-earth